Role of Phosphate Chain Mobility of MgATP in Completing the 3-Phosphoglycerate Kinase Catalytic Site: Binding, Kinetic, and Crystallographic Studies with ATP and MgATP†

Beáta Flachner,‡,§ Zoltán Kovári,*,§,||,Δ Andrea Varga,‡ Zoltán Gugolya,⊥ Ferenc Vonderviszt,⊥ Gábor Náray-Szabó,@ and Mária Vas*,‡

Institute of Enzymology, Biological Research Center, Hungarian Academy of Sciences, P.O. Box 7, H-1518 Budapest, Hungary, Protein Modeling Group, Hungarian Academy of Sciences-Eötvös Loránd University, Pázmány Péter st. 1A, H-1117 Budapest, Hungary, Department of Computer Assisted Drug Discovery, Gedeon Richter Ltd., P.O. Box 27, H-1475 Budapest 10, Hungary, Department of Chemical Information Technologies, Budapest University of Technology and Economics, H-1111, Budapest, Szt. Gellért tér 4, and Department of Physics, University of Veszprém, P.O. Box 158, H-8201 Veszprém, Hungary

Received June 16, 2003; Revised Manuscript Received November 24, 2003

ABSTRACT: The complexes of pig muscle 3-phosphoglycerate kinase with the substrate MgATP and with the nonsubstrate Mg^{2+}-free ATP have been characterized by binding, kinetic, and crystallographic studies. Comparative experiments with ADP and MgADP have also been carried out. In contrast to the less specific and largely ionic binding of Mg^{2+}-free ATP and ADP, specific occupation of the adenosine binding pocket by MgATP and MgADP has been revealed by displacement experiments with adenosine and anions, as well as supported by isothermal calorimetric titrations. The Mg^{2+}-free nucleotides similarly stabilize the overall protein structure and restrict the conformational flexibility around the reactive thiol groups of helix 13, as observed by differential scanning microcalorimetry and thiol reactivity studies, respectively. The metal complexes, however, behave differently. MgADP, but not MgATP, further increases the conformational stability with respect to its Mg^{2+}-free form, which indicates their different modes of binding to the enzyme. Crystal structures of the binary complexes of the enzyme with MgATP and with ATP (2.1 and 1.9 Å resolution, respectively) have shown that the orientation and interaction of phosphates of MgATP largely differ not only from those of ATP but also from the previously determined ones of either MgADP [Davies, G. J., Gamblin, S. J., Littlechild, J. A., Dauter, Z., Wilson, K. S., and Watson, H. C. (1994) *Acta Crystallogr. D50*, 202−209] or the metal complexes of AMP-PNP [May, A., Vas, M., Harlos, K., and Blake, C. C. F. (1996) *Proteins 24*, 292−303; Auerbach, G., Huber, R., Grattinger, M., Zaiss, K., Schurig, H., Jaenicke, R., and Jacob, U. (1997) *Structure 5*, 1475−1483] and are more similar to the interactions formed with MgAMP-PCP [Kovári, Z., Flachner, B., Náray-Szabó, G., and Vas, M. (2002) *Biochemistry 41*, 8796−8806]. Mg^{2+} is liganded to both β- and γ-phosphates of ATP, while β-phosphate is linked to the conserved Asp218, i.e., to the N-terminus of helix 8, through a water molecule; the known interactions of either MgADP or the metal complexes of AMP-PNP with the N-terminus of helix 13 and with Asn336 of β-strand J are absent in the case of MgATP. Fluctuation of MgATP phosphates between two alternative sites has been proposed to facilitate the correct positioning of the mobile side chain of Lys215, and the catalytically competent active site is thereby completed.

Kinases essentially use the metal complexes of ATP and ADP as substrates. This was also recognized for the reaction catalyzed by 3-phosphoglycerate kinase (PGK)[1] (*1*−*3*). In general, there are still open questions concerning the role of the metal ion in catalysis. Its possible roles, such as shielding the negative charges of the phosphates, assisting in the development of negative charge on the leaving group, stabilizing the transition state, or orienting the reactive partners in the optimal alignment (*4*−*6*), must be investigated in individual cases.

According to crystallographic studies, PGK consists of two domains. The C-terminal domain binds the nucleotide,

† The financial support provided by OTKA Grants T043446, T034994, and T042933 of the Hungarian National Research Fund is gratefully acknowledged.

* To whom correspondence should be addressed. M.V.: Institute of Enzymology, BRC, Hungarian Academy of Sciences, P.O. Box 7, H-1518 Budapest, Hungary; telephone, 36 1 279 3152; fax, 36 1 466 5465; e-mail, vas@enzim.hu. Z.K.: Department of Computer Assisted Drug Discovery, Gedeon Richter Ltd., P.O. Box 27, H-1475 Budapest 10, Hungary; telephone, 36 1 431 5679; fax, 36 1 432 6002; e-mail, z.kovari@enzim.hu.

‡ Hungarian Academy of Sciences.

§ These authors contributed equally to this work.

|| Gedeon Richter Ltd.

Δ Budapest University of Technology and Economics.

⊥ University of Veszprém.

@ Hungarian Academy of Sciences-Eötvös Loránd University.

[1] Abbreviations: PGK, 3-phospho-D-glycerate kinase or ATP:3-phospho-D-glycerate 1-phosphotransferase (EC 2.7.2.3); GAPDH, D-glyceraldehyde-3-phosphate dehydrogenase (EC 1.2.1.12); 3-PG, 3-phospho-D-glycerate; 1,3-BPG, 1,3-bisphosphoglycerate; AMP-PNP, β,γ-imidoadenosine 5′-triphosphate; AMP-PCP, β,γ-methyleneadenosine 5′-triphosphate; Nbs_2, Ellmann's reagent [5,5′-dithiobis(2-nitrobenzoic acid)]; ITC, isothermal titration microcalorimetry; DSC, differential scanning microcalorimetry.

10.1021/bi035022n CCC: $27.50
Published on Web 03/04/2004

MgADP (*7*), or MgATP (*8*), and the N-terminal domain binds 3-PG (*9*) or, possibly, 1,3-bisphosphoglycerate. A growing body of evidence suggests that during catalysis, the domains move toward each other to bring the substrates into the proper vicinity for phosphotransfer (*8*, *10*−*15*). Although a single nucleotide site of PGK has been determined by X-ray crystallography with the enzyme from various sources (*7*, *8*, *10*, *16*−*20*), binding studies with the solubilized enzyme have not led to such uniform results. The existence of an additional secondary nucleotide site has been proposed from equilibrium dialysis (*21*), gel filtration (*22*, *23*), chemical modification (*24*), and NMR studies (*25*−*29*). In contrary, other NMR (*22*, *30*), spectrophotometric (*31*), fluorimetric titration (*32*−*34*), and thiol reactivity (*20*, *35*) studies as well as direct equilibrium dialysis experiments (*36*, *37*) could be satisfactorily fitted to a single-nucleotide site model. The variation of the published K_d values of nucleotide binding (*26*, *28*, *29*, *31*, *32*, *38*) further increases these uncertainties.

A high-resolution crystal structure exists for only MgADP binding where the nucleotide is bound to the PGK from *Bacillus stearothermophilus* and clearly shows interactions of Mg^{2+} with both α- and *β*-phosphates of ADP and with a conserved aspartate side chain [Asp352 in the *B. stearothermophilus* PGK (*7*), corresponding to Asp374 in the pig muscle enzyme]. This structure provides an explanation for the strengthening of ADP binding by Mg^{2+}. This type of Mg^{2+} chelation to ADP is consistent with other crystallographic (*8*, *16*, *19*), NMR (*38*, *39*), and EPR (*40*) investigations. Equilibrium dialysis studies have confirmed the role of Mg^{2+} in ADP binding, but no such effect was detectable for ATP binding (*36*, *37*). These observations and other studies, such as thiol reactivity (*35*) and fluorimetry (*33*, *34*) studies, may indicate different binding modes of MgADP and MgATP.

The position of the chelating Mg^{2+} and that of the phosphate chain are, however, still equivocal for the bound MgATP. Preliminary X-ray studies upon diffusion of MgATP into the pregrown crystals of horse (*8*) and yeast (*16*) PGKs indicate interaction of only the α-phosphate with the ϵ-amino group of Lys219 (pig muscle PGK numbering), characteristic also for the bound MgADP (*7*), but no interacting side chains close either to the *β*- and *γ*-phosphates or to the metal ion (located in the vicinity of the *γ*-phosphate) have been observed. Up to now, however, no crystal structure has been determined for the true complex cocrystallized with MgATP. Kinetic studies with stereoselective ATP analogues (*41*, *42*) and NMR investigations (*39*) also gave equivocal results with regard to the metal coordination to the ATP phosphates. In addition, a remarkable coordination pattern of the metal ion has been observed from ^{31}P NMR studies with $Rh(H_2O)_n$-ATP in the presence of the substrate, 3-phosphoglycerate (3-PG) (*43*). Namely, the metal ion is coordinated to both ligands, suggesting that it may help to align the two substrates for the phosphotransfer.

Crystallographic studies with the ATP analogue AMP-PNP (*13*, *17*, *18*) have shown coordination of the metal ion to all three phosphates, but not to the protein, while our study with another analogue, AMP-PCP, has shown Mg^{2+} coordination to only the *β*-phosphate (*20*). Thus, neither of the structural observations with the analogues resembles the initially observed coordination with ATP (*8*, *16*).

The conformation of the nucleotide phosphates and their interaction with the protein are also contradictory for MgATP. The interaction of the α-phosphate of ATP with the side chain of Lys219, mentioned above, has been confirmed by crystallographic studies with both analogues of AMP-PNP and AMP-PCP (*13*, *17*, *18*, *20*), as well as by solution kinetic studies (*44*). However, the conformation of the phosphate chain and location of the phosphates of AMP-PNP and AMP-PCP are completely different. While that of AMP-PNP resembles the location of ADP phosphates close to the N-terminus of helix 13, here without involvement of Mg^{2+} (*13*, *17*, *18*), the phosphates of AMP-PCP bind to an alternative site at the N-terminus of helix 8, through the metal ion (*20*). Solution of the complete NMR structures of both the bound MnADP and MnATP (*45*) has not solved the above uncertainties. The nucleotide conformations have been shown to be different not only from each other but also from the crystallographic conformations of *both* bound nucleotides (*7*, *8*, *16*, *19*).

To compare the binding characteristics of the two nucleotide substrates, MgATP and MgADP binding to PGK, as well as their dependence on the complexing metal ion, in this work various complementary methodologies (such as precision isothermal calorimetric titration, competitive displacement by analogues, enzyme kinetics, differential scanning calorimetry, thiol reactivity, and X-ray crystallography) have been applied. These studies may also allow exclusion of any differences, which originated from the inherent properties of the two physical states (solution and crystal) of the protein.

On the basis of these results, we aimed to answer the following specific questions. (i) How do the orientation and interactions of phosphates of bound MgATP relate to those extremely different orientations and interactions observed in the previous crystal structures with bound Mg(Mn)AMP-PNP (*13*, *17*, *18*) and with MgAMP-PCP (*20*)? (ii) Is there any special role for the metal ion, in addition to the generally expected ones, in formation of the catalytic complex of PGK with each nucleotide substrate? (iii) If MgATP phosphates bind to the alternative site, similar to that of MgAMP-PCP (*20*), what would be the possible catalytic relevance of this binding mode in light of the suggested catalytic mechanism (*7*, *8*, *16*, *19*) and the known active site geometry (*13*, *17*, *18*) of PGK?

MATERIALS AND METHODS

Enzymes and Chemicals. PGK (EC 2.7.2.3) was isolated from pig muscle as described by Harlos et al. (*9*) and stored as a microcrystalline suspension in the presence of ammonium sulfate and 2 mM dithiothreitol. Its activity, determined by D-3-phosphoglycerate and MgATP, varied between 500 and 700 kat/mol. Glyceraldehyde-3-phosphate dehydrogenase (GAPDH, EC 1.2.1.12) was prepared from pig muscle (*46*).

Lactate dehydrogenase, pyruvate kinase, and the sodium salts of 3-PG, NADH, ATP, ADP, AMP, adenosine, NADH, and phosphoenolpyruvate were Boehringer products. The complexes of MgATP and MgADP were formed by adding $MgCl_2$ (Sigma) in a high molar excess, which assured a practically complete saturation on the basis of dissociation constants of 0.1 and 0.6 mM, respectively, which were averaged from the literature (*1*, *47*−*50*). Mg complexes of AMP-PNP and AMP-PCP have been produced in a similar

way on the basis of K_d values of 0.09 and 0.08 mM, respectively (*51*). All other chemicals were reagent-grade commercial preparations. The Ellmann's reagent (Nbs2) and iodoacetamide were obtained from Serva. The latter was recrystallized from carbon tetrachloride before being used.

Preparation of Enzyme Solutions. Crystals of PGK were dissolved in 20 mM Tris-HCl buffer (pH 7.5) containing 1 mM dithiothreitol, and the mixture was dialyzed either against the same buffer (for enzyme kinetic measurements) or in 50 mM Tris-HCl buffer (pH 7.5) to remove $(NH_4)_2SO_4$. The GAPDH solution was desalted in the same way under the lower-ionic strength conditions. For thiol reactivity measurements, 1 mM dithiothreitol was omitted from the dialysis buffer, but it contained 1 mM EDTA. For isothermal calorimetric studies, the dialysis buffer contained 5 mM 2-mercaptoethanol in place of dithiothreitol. For determining protein concentrations, A_{280} values of a 1 mg/mL solution of PGK and GAPDH were taken to be 0.69 (*52*) and 1.0 (*53*), respectively, for a 1 cm path length. The molecular mass of PGK was taken to be 44.5 kDa (*54*).

Enzyme Kinetic Studies. The activity of PGK was measured with 3-PG and MgATP as substrates in 20 mM Tris-HCl buffer (pH 7.5) and 1 mM dithiothreitol at 20 °C. In the assay, oxidation of NADH by the reaction product in the presence of GAPDH was followed by spectrophotometry at 340 nm as described by Tompa et al. (*35*). The double-inhibition experiments were carried out in the simultaneous presence of two different inhibiting molecules at a constant concentration of the substrates. At varying concentrations of the first inhibitor, the activity measurements were repeated in the absence and presence of constant concentrations of the second inhibitor. In the experiments carried out in the presence of phosphate, pyrophosphate, and citrate, the complexation properties of these anions with Mg^{2+} were taken into account with K_d values of 15.8, 0.66 (*55*), and 0.43 mM (*56*), respectively. Thus, the distribution of Mg^{2+} between anions and the nucleotides has been calculated, and only the resulting concentrations of the metal−nucleotide complexes have been considered in the kinetic experiments. The results have been analyzed using the method from ref *57*.

Kinetic Measurements of Thiol Reactivity toward Nbs_2. The experiments with PGK were carried out in 50 mM Tris-HCl buffer (pH 7.5) containing 1 mM EDTA at 20 °C in the absence and presence of substrates and their analogues. The reaction was started with an equimolar amount or excess of Nbs_2 and followed by measuring the change in absorbance at 412 nm, as described previously (*58*). During the time of the reaction of the freely accessible fast-reacting thiols (two per mole of PGK), the reaction of the other inaccessible thiols (five per mole) is negligible. The fast-reacting thiols belong to Cys378 and Cys379, respectively, as identified later (*59*, *60*). The amount of thiols that reacted was calculated by using an ϵ_{412} of 14 150 M^{-1} cm^{-1} (*61*), and approximately 1.5−2.0 mol per mole of fast-reacting thiols was found.

Determination of Dissociation Constants for Binding of the Nucleotide to PGK. In all calculations, a 1:1 binding stoichiometry for nucleotides is assumed according to the binding equation

$$Y = \frac{[EN]}{[E]_{total}} = \frac{[N]}{K_d + [N]} \quad (1)$$

where Y is the fractional saturation, $[E]_{total}$ represents the total enzyme concentration that equals the total concentration of sites which can be filled with the ligand N, [EN] is the concentration of the enzyme−ligand complex, and K_d is the dissociation constant. While Y varies from 0 to 1, [N] varies from 0 to ∞.

The dissociation constants (K_d) of the nucleotides (N) or their apparent values (K_{dApp}) in the presence of various competitors (L) were obtained by determining the rate constant of thiol modification with Nbs_2 at different concentrations of the nucleotide, in both the absence and presence of the investigated competitor. As described earlier, the level of protection against modification is proportional to the amount of enzyme−ligand (here EN) complex formed, which allows calculation of K_d by fitting the experimental points with the following equation (*20*), which in principle can be derived from eq 1:

$$k_{measured} = k_{max} - \frac{(k_{max} - k_{min})[N]}{K_d + [N]} \quad (2)$$

where k_{max}, k_{min}, and $k_{measured}$ are the rate constants of thiol modification in the absence of, at an infinite concentration, and at an intermediate concentration, respectively, of the nucleotide applied in the experiment and [N] is the free nucleotide concentration in the reaction mixture (it can be replaced by the total concentration as the enzyme-bound nucleotide is negligible under the experimental conditions). In the presence of competitors, K_d in eq 2 is replaced with K_{dApp}. The fractional saturation (Y) in this case can be expressed as

$$Y = \frac{k_{max} - k_{measured}}{k_{max} - k_{min}} \quad (3)$$

In case of pure competitive displacement, the following relationship holds between the real K_d and its apparent value, K_{dApp}:

$$K_{dApp} = K_d\left(1 + \frac{[L]}{K_L}\right) \quad (4)$$

where [L] is the concentration of the competitor and K_L is the dissociation constant for the binding to the enzyme in the absence of the nucleotide.

Thus, if we assume a complete displacement by the competitor, L, and by substitution of K_{dApp} from eq 4 into eq 1 in place of K_d, a theoretical dependence of the fractional saturation by the nucleotide, Y, can be calculated as a function of [L], at any constant value of [N]:

$$Y = \frac{[N]}{K_d\left(1 + \frac{[L]}{K_L}\right) + [N]} \quad (5)$$

This relationship can be greatly simplified, and becomes independent of the K_d value of the actual ligand, N, if [N] is expressed in terms of CK_d, where C is a constant. For example, in the case of the theoretical curve starting (at [L]

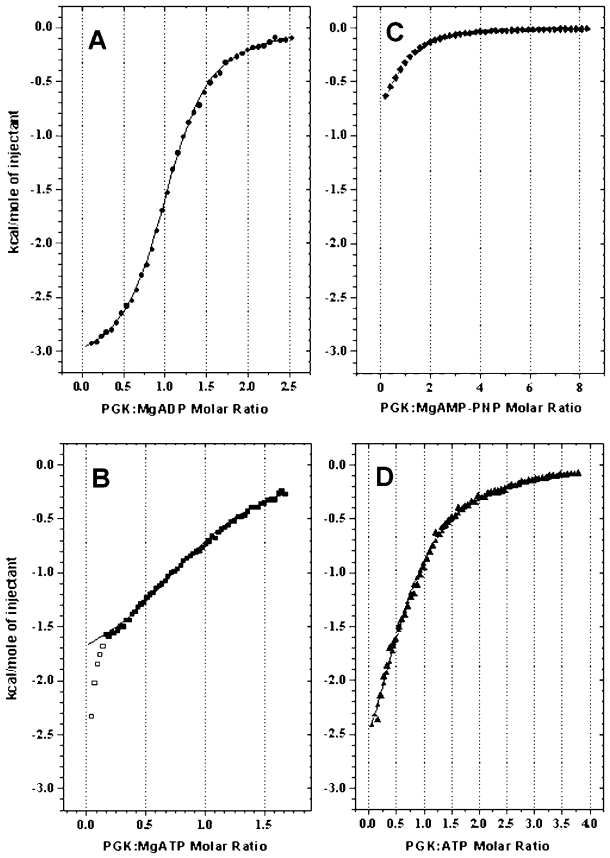

FIGURE 1: ITC titrations of PGK with various nucleotides. A PGK solution (0.5−1.5 mM) was placed in the cell either in the absence or in the presence of 12−25 mM $MgCl_2$ and titrated with 8.5 mM MgADP (A, ●), 10 mM MgATP (B, ■), 20 mM MgAMP-PNP (C, ◆), or free ATP (D, ▲). The best fits of the data to a model with a single binding site obtained by nonlinear regression are shown as solid lines. In panel B, the initial few points (□) at very low PGK:MgATP molar ratios were attributed to a heat change of unknown origin, most probably, not characteristic for PGK. These points have been omitted before fitting of the data because all the points in panel B could not be satisfactorily fitted by a single-site model. The thermodynamic data that were obtained are summarized in Table 2.

= 0) from a $Y = 0.5$ saturation, which corresponds to [N] = K_d, this value of [N] is kept constant (i.e., here $C = 1$) throughout varying [L] values and the following relationship is valid:

$$Y = \frac{K_d}{K_d\left(1 + \frac{[L]}{K_L}\right) + K_d} = \frac{1}{2 + \frac{[L]}{K_L}} \qquad (6)$$

In this way, a series of theoretical curves can be constructed at various constant values of [N], as a function of the competitor concentration, [L]. The advantage of these curves is the fact that their shape does not depend on the K_d value of the ligand, N. Thus, the ability of the same competitor, L, to displace two different ligands, N_1 and N_2, can be directly compared (cf. Figure 2), and only the ratio of concentrations of N_1 and N_2 should be chosen according to the ratio of their respective dissociation constants:

$$\frac{[N_1]}{[N_2]} = \frac{K_{d1}}{K_{d2}} \qquad (7)$$

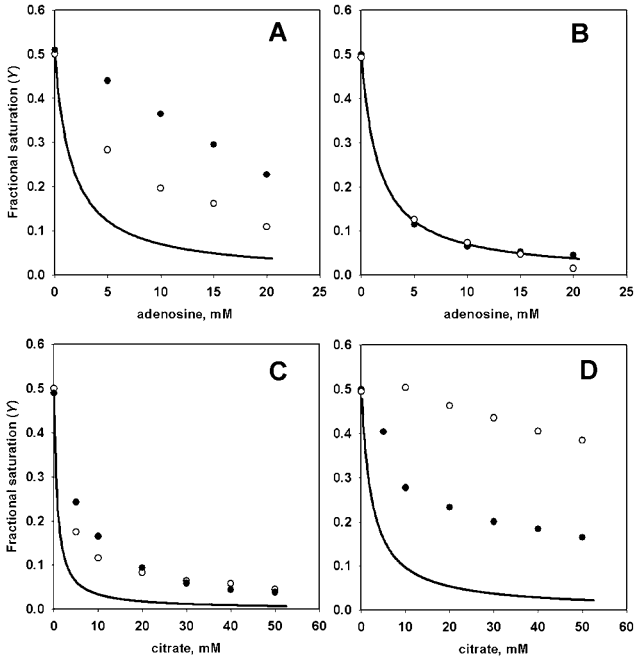

FIGURE 2: Displacement of the bound nucleotides by adenosine or citrate. The fractional saturations (Y) of PGK (as given by eq 3) with ATP (●) and ADP (○) were determined by the indirect method using Nbs_2 in the presence of a constant concentration of the nucleotides (equal to the corresponding K_d values, cf. Table 3) and at various concentrations of competing ligands, adenosine (A and B) and citrate (C and D), indicated in the abscissa. All experiments were carried out in the absence (A and C) and presence (B and D) of excess Mg^{2+}. The concentration of Mg^{2+} was applied in the range of 12.5−65.0 mM, depending on the concentration of citrate, to ensure saturation of all nucleotides with Mg^{2+}. Theoretical dependences of Y as a function of the increasing concentration of the competing ligands (solid lines) were calculated, using eq 6 (for when [N] = K_d), which is the simplified form of the more general eq 5.

Kinetic Measurements of Alkylation by Iodoacetamide. PGK was alkylated with iodoacetamide under pseudo-first-order conditions, i.e., with a high molar excess of the alkylating agents, in 50 mM Tris-HCl buffer at pH 7.5 and 20 °C. Under these conditions, the two reactive cysteinyl residues are selectively modified, which is accompanied by the loss of enzyme activity (*62*). Kinetics of alkylation were followed by determining residual PGK activity in aliquots withdrawn from the reaction mixture at appropriate time points (*35*). The concentration of iodoacetamide was determined by using an ϵ_{275} molar absorption coefficient of 373 M^{-1} cm^{-1} (*63*).

Isothermal Calorimetric Titration (ITC) Experiments. ITC was performed using a MicroCal VP-ITC type microcalorimeter (MicroCal Inc.) at 20 °C. Temperature equilibration prior to experiments was allowed for 1−2 h. All solutions were thoroughly degassed before being used by stirring under vacuum. Protein and the titrating ligand samples were prepared in the same dialysis buffer. The pH of nucleotide solutions was carefully checked and, if required, adjusted to pH 7.5. A typical titration experiment consisted of consecutive injections of 5 μL of the titrating ligand (approximately in 60 steps), at 3 min intervals, into the protein solution in the cell with a volume of 1.42 mL. The titration data were corrected for the small heat changes observed in control titrations of ligands into the buffer. The data were analyzed

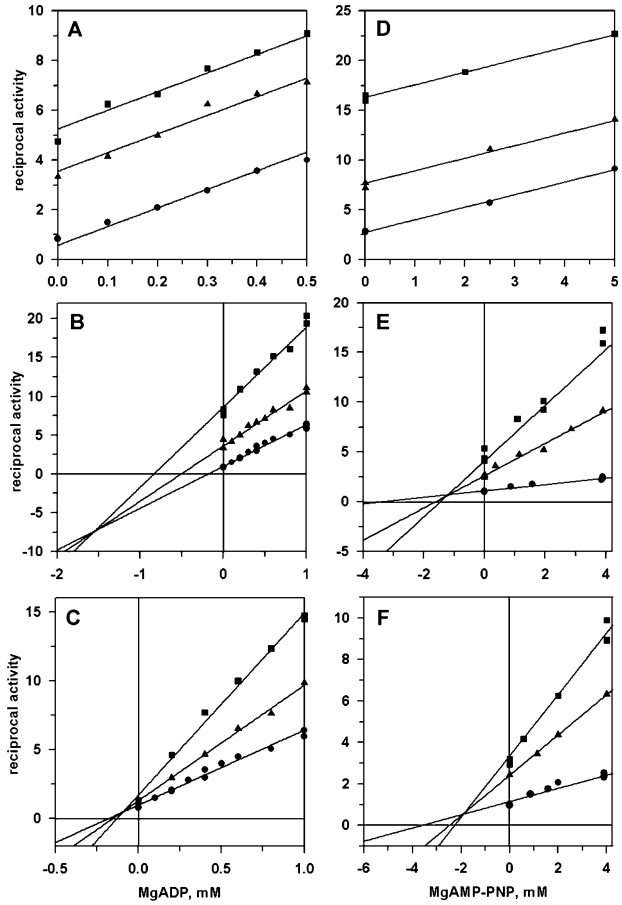

FIGURE 3: Double inhibition by various pairs of inhibitors. The experiment was carried out with 50 nM enzyme, 0.5 mM 3-PG (except for panel D, where 10 mM was applied), and 0.5 (A−C) or 0.15 mM ATP (D−F). All mixtures contained 12.5 mM $MgCl_2$. Activity was determined as a function of either the MgADP (A−C) or MgAMP-PNP (D−F) concentration. The measurements were taken in the absence of a second inhibitor (■) as well as in the presence of 10 (▲) and 20 mM adenosine (●) (A), 35 (▲) and 45 mM pyrophosphate (●) (B), 20 (▲) and 50 mM 2-phosphoglycolate (●) (C), 10 mM (▲) adenosine and 0.75 mM MgADP (●) (D), 25 (▲) and 30 mM pyrophosphate (●) (E), and 70 (▲) and 100 mM 2-phosphoglycolate (●) (F) and plotted according to the method of Yonetani and Theorell (*57*).

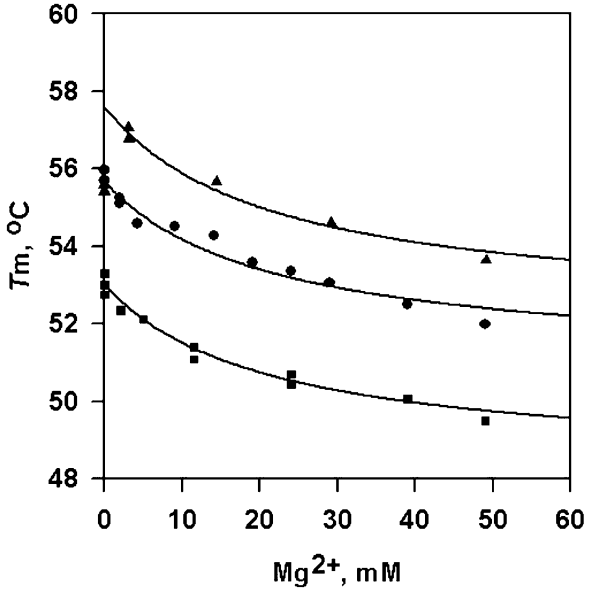

FIGURE 4: Effect of nucleotides on the thermal unfolding of PGK. DSC melting experiments were carried out in the presence of different concentrations of Mg^{2+} both in the absence of nucleotide (■) and in the presence of 10 mM ATP (●) or 10 mM ADP (▲). The Mg^{2+} concentrations, given on the abscissa, were obtained by subtracting the concentration of Mg^{2+} bound to ATP or ADP and to $[EDTA]^{4-}$, present in the medium, from its total concentration. For calculation of the concentration of Mg^{2+} bound to these compounds, K_d values of 0.1, 0.6, and 2.5×10^{-9} mM, respectively, were used. The concentration of the fully dissociated form of EDTA, $[EDTA]^{4,-}$ at pH 7.5 was calculated by using the known acid dissociation constants of EDTA. The solid lines represent the best fit of the experimental points to eq 3, given in Materials and Methods. The fitting yielded a K of 21.3 ± 5.0 mM, characteristic of Mg^{2+} binding to PGK, for all three sets of data. In this way, the experimental points could be extrapolated to an Mg^{2+} concentration of zero; i.e., T_{max} values without the effect of the metal ion were obtained as follows: 53.0 ± 0.06, 55.6 ± 0.32, and 57.6 ± 0.36 °C for the substrate-free PGK, the complexes with MgATP, and the complexes with MgADP, respectively. The measured T_m values in the absence of Mg^{2+} are 53.0 ± 0.2, 55.8 ± 0.2, and 55.7 ± 0.2 °C for free PGK and its complexes with ATP and ADP, respectively.

by assuming a 1:1 binding stoichiometry using MicroCal Origin 5.0.

Differential Scanning Calorimetric (DSC) Experiments. Heat-induced unfolding of PGK was investigated by DSC experiments. All measurements were performed in a MicroCal VP-DSC type microcalorimeter (MicroCal Inc.) with a cell volume of 0.51 mL at a constant scan rate of 60 °C/h. The protein concentration was 0.13 mg/mL (0.003 mM) in all experiments. All the samples were carefully degassed before the experiments. The data were analyzed using the online computer of the equipment with the aid of MicroCal Origin 5.0. The melting temperature (T_m) has been determined after subtraction of the instrumental baseline.

The dependence of T_m on the concentration of Mg^{2+} (cf. Figure 4) was taken into account by fitting the experimental values to the following equation (similar to eq 2):

$$T_{measured} = T_{max} - \frac{(T_{max} - T_{min})[Mg^{2+}]}{K + [Mg^{2+}]} \qquad (8)$$

where T_{max}, T_{min}, and $T_{measured}$ are the melting temperatures of PGK in the absence of, at an infinite concentration, and at an intermediate concentration, respectively, of Mg^{2+}, used in the experiments, K is considered a dissociation constant for binding of Mg^{2+} to PGK, and Y is the fractional saturation.

Crystallization. Single crystals of the binary complexes with ATP and MgATP were grown in hanging drops, at 15 °C, within ~2 weeks. The protein solution (14 mg/mL) at pH 8.0 contained either 10 mM ATP in 1.4 M NaK-phosphate buffer or 10 mM ATP and 12 mM $MgCl_2$ in 0.6 M sodium citrate buffer. The reservoir solutions contained the same buffers described above, but the precipitant concentrations were higher: 2.1 M NaK-phosphate and 1.2 M sodium citrate, respectively. The characteristics of the crystals obtained and the data collection statistics are summarized in Table 1.

Data Collection and Refinement. Data collection and refinement were carried out in the same way for both complexes. X-ray data were collected at 20 °C from single crystals with dimensions of 0.6 mm × 0.2 mm × 0.2 mm (PGK·MgATP) and 0.8 mm × 0.4 mm × 0.3 mm (PGK·

Table 1: Data Collection and Refinement Statistics

	ATP	MgATP
data collection		
space group	$P2_1$	$P2_1$
unit cell dimensions		
a (Å)	36.2	36.2
b (Å)	106.4	106.5
c (Å)	51.1	51.1
β (deg)	97.8	97.6
no. of unique reflections	26788	20849
completeness (%)	92.1	93.2
R_{merge} (%)[a]	8.7	16.8
refinement		
resolution (Å)	34.00−1.9	27.00−2.1
R (%)[b]	18.72	17.31
R_{free} (%)[b]	23.51 (0.1)	23.30 (0.1)
B-factors (Å^2)		
mean[c]	26.31 (3255)	23.95 (3242)
protein main chain[c]	24.93 (1664)	22.39 (1664)
protein side chain[c]	26.72 (1397)	23.90 (1361)
water molecules[c]	33.14 (158)	35.12 (185)
phosphate[c]	44.57 (5)	−
nucleotide[c]	44.27 (31)	42.48 (32)
bond length rmsd (Å)[d]	0.006	0.007
bond angle rmsd (deg)[d]	1.15	1.23
torsion angle rmsd (deg)[d]	26.33	25.94
improper torsion angle rmsd (deg)[d]	0.64	0.60
Ramachandran plot[d]		
core (%)	90.8	90.1
allowed (%)	8.9	9.6
generously allowed (%)	0.3	0.3
disallowed (%)	0	0

[a] $R_{merge} = \sum_{hkl}\sum_i|\langle I(hkl)\rangle - I(hkl)_i|/\sum_{hkl}\langle I(hkl)\rangle$, where $I(hkl)_i$ is the measured diffraction intensity and $\langle I(hkl)\rangle$ is the mean intensity. [b] *R*-factor $= \sum_{hkl}|F_{obs}(hkl) - F_{calc}(hkl)|/\sum_{hkl}|F_{obs}(hkl)|$. R_{free} is the *R*-factor for a test set comprising 10% of the data selected randomly. [c] The numbers in parentheses denote the number of non-hydrogen atoms. [d] Stereochemistry was assessed with X-PLOR (*67*) and PROCHECK (*76*).

ATP) in 3° oscillation images using a Rigaku RU200 rotating anode X-ray generator and a Rigaku Raxis II image plate detector. The data were processed with the MOSFLM package (*64*). Molecular replacement was carried out with AMoRe (*65*) of Collaborative Computing Project Number 4 (*66*) using the PGK·MgAMP-PCP·3-PG structure (*20*) as a template, and bound ligands and water molecules were deleted from the coordinate file that was used. Refinement was carried out in cycles of the X-PLOR package (*67*) together with manual rebuilding of the model at the end of each cycle using O (*68*). A random set of the reflections (10%) was excluded from the refinement and was used to calculate R_{free}. The $2F_o - F_c$ electron density map calculated at the first stage of refinement clearly showed the position of the bound ligands and the open domain conformations. This was followed by cycles of positional refinement, simulated annealing, and individual anisotropic *B*-factor refinement. After the first cycle of refinement, the nucleotides were included in the models. After additional refinement cycles, water molecules were added to (i) stereochemically acceptable positions suggested by Waterpick (in X-PLOR) and (ii) positions with acceptable electron density. Bulk solvent corrections were applied at a later stage in the refinement. Only side chains with acceptable density were included in the model, while side chains with unacceptable density were shortened according to the electron density map. Main chain atoms are well-defined by the electron density in both cases; however, residues of a surface loop (amino acids 28−32) have poor side chain densities. Other poor side chain densities were observed for only individual residues. Alternative side chain conformations of some residues were refined.

Refinement of the structures is greatly aided by the information deduced from the TIGR gene expression database (*69*) about the amino acid sequence of pig muscle PGK. The sequence of this PGK was assigned previously (*9*) on the basis of the published horse muscle PGK sequence (*8*) and the observed electron density maps of the crystal structures (*10*). The new sequence differed from the formerly assigned ones in only some nonconserved surface residues. The differences were checked carefully in the electron density maps of the structures presented here, which resulted in an improved sequence for pig muscle PGK.

For molecular graphics, Insight II (Biosym/MSI, San Diego, CA) and Sybyl 6.9 (Tripos Inc., St. Louis, MO) were used. The protein coordinates have been deposited in the Protein Data Bank with accession numbers 1VFC and 1VFD for PGK·MgATP and PGK·ATP complexes, respectively.

Table 2: Thermodynamic Parameters of Nucleotide Binding to PGK[a]

nucleotide	K_a ($\times 10^{-5}$ M^{-1})	K_d (mM)	ΔH (cal/mol)	$T\Delta S$ (cal/mol)	ΔG (cal/mol)
MgADP	1.86 ± 0.22	0.054	−3178 ± 49	2533 ± 26	−5718
MgATP	0.38 ± 0.05	0.263	−1355 ± 280	3302 ± 78	−4797
MgAMP-PNP	0.28 ± 0.06	0.357	−1147 ± 145	3627 ± 158	−4619
ATP	0.35 ± 0.04	0.286	−3939 ± 184	996 ± 197	−4748

[a] The values are obtained by fitting the ITC titration data by applying the single-site binding model. The values of ΔG were calculated from the association constants (K_a). For comparison to the data of Table 3, the values of the respective dissociation constants (K_d), as derived from K_a, are also given. For MgAMP-PNP binding, the K_d of 0.41 ± 0.08 mM was obtained from an independent experiment (*20*). The values are means ± the experimental error from two to five individual measurements. *T* is the temperature in kelvin (1 cal = 4.186 J).

RESULTS

Nucleotide Binding to PGK Characterized by ITC Titrations. Figure 1 illustrates typical titrations of PGK with the nucleotide substrates MgADP (A) and MgATP (B) as well as titrations with the analogue MgAMP-PNP (C) and Mg^{2+}-free ATP (D). In all cases, the best fit to the experimental data was obtained by assuming a 1:1 stoichiometry of binding, in agreement with previous equilibrium dialysis (*36*) and crystallographic data showing only a single molecule of bound nucleotide either for MgADP (*7*) or for Mg/MnAMP-PNP (*13*, *17*). Although the results obtained for titrations with MgATP include some uncertainty (cf. the legend of Figure 1), the illustrated way of data fitting is consistent with both the 1:1 stoichiometry and the known K_d values determined previously (*34*, *36*, *37*). The thermodynamic parameters of the binding are summarized in Table 2. The stronger interaction of MgADP with PGK, compared to that of MgATP (*34*, *36*, *37*), is clearly confirmed. In thermodynamic terms, MgADP binding is a mostly enthalpy-driven exothermic process, compared to the less exothermic binding of MgATP. On the other hand, binding of MgATP itself is mainly driven by favorable entropy changes, which (among other factors) may be due to the increased mobility of its phosphates, in correlation with other experimental data below. The values obtained with the MgAMP-PNP analogue are very similar to those with MgATP. Remarkable differ-

Table 3: Dissociation Constants for Binding of the Nucleotide and of the Ligands Used in the Displacement Experiments[a]

	K_d (mM)			
	ATP	ADP	adenosine	citrate
no Mg^{2+}	0.23 ± 0.06	0.34 ± 0.05	0.81 ± 0.13	0.36 ± 0.05
	0.21 ± 0.03[b]	0.27 ± 0.04[b]		
molar excess of $Mg^{2=}$	0.23 ± 0.05	0.05 ± 0.01	0.81 ± 0.13	1.20 ± 0.26
	0.23 ± 0.03[b,c]	0.06 ± 0.0[b,c]		

[a] K_d values have been determined from thiol reactivity measurements as described in Materials and Methods. [b] From ref *36*. [c] From ref *37*.

ences have been observed, however, due to the presence or absence of Mg^{2+}: the binding of ATP itself is an enthalpy-driven process (possibly due to stronger ionic interactions), in contrast to the entropy-driven binding of MgATP. This is an interesting example of comparable binding affinities of two ligands (ATP and MgATP), as established also in previous binding data (*36*), arising from different ratios of the binding enthalpy (ΔH) and entropy (ΔS).

Effects of Adenosine and Anions on Nucleotide Binding. To explore the relative contribution of the hydrophobic adenosine moiety and that of the anionic phosphate chain of the nucleotides to the binding to PGK, displacement experiments with adenosine and the anions (citrate or pyrophosphate) have been carried out with ATP and ADP, in both the absence and presence of Mg^{2+}. As described in Materials and Methods, the fractional saturation (cf. eq 3) at a constant concentration of the investigated nucleotide has been determined by thiol reactivity studies as a function of the concentration of each competing ligand (cf. Figure 2). For this, at first the dissociation constants of each individual nucleotide in the absence of the competitor and of each competitor in the absence of nucleotide have been determined by the same method, in separate experiments. The resulting K_d values are summarized in Table 3 and agree satisfactorily with the previously determined equilibrium dialysis data. Using these values, the theoretical dependence of fractional saturation by the nucleotides on the concentration of the competing ligands has been calculated for the case of pure competition, as outlined in Materials and Methods (cf. eq 6), and also plotted in Figure 2. Comparison of these curves to the experimental points clearly shows that adenosine can displace completely either the bound MgATP or MgADP (Figure 2B), while it can only partially displace the bound ATP or ADP (Figure 2A). On the other hand, no complete displacement can be observed by citrate in either case; however, it displaces ATP or ADP (Figure 2C) significantly better than MgATP or MgADP (Figure 2D). It is also notable in the latter case that citrate can only hardly displace MgADP, compared to MgATP, in agreement with the known strengthening effect of Mg^{2+} on ADP binding. Qualitatively, the same results were obtained when pyrophosphate was applied in place of citrate. In summary, the displacement experiments have revealed less specific and largely ionic interactions of the Mg^{2+}-free nucleotides with PGK, while both MgATP and MgADP bind exclusively to the specific adenosine binding pocket.

Double-Inhibition Experiments with Nucleotide Analogues and Adenosine or Anions. To characterize and compare the interactions of the nucleotides with the functioning enzyme, the kinetic approach of double-inhibition studies has been applied as illustrated by the Yonetani−Theorell plots (*57*) in Figure 3. In one series of experiments, MgADP (as the inhibitory product) has been added to the activity assay mixture together with another inhibitor [adenosine (A), a multivalent anion (B), or a 3-PG analogue (C)]. In another series of experiments, a nonreactive analogue of MgATP, MgAMP-PNP (in some cases MgAMP-PCP) (*51*), has been added at the same time as the same second inhibitor [adenosine (D), anion (E), or 3-PG analogue (F)]. The parallel lines in panels A and D of Figure 3 indicate that the inhibitory effects of MgADP, MgAMP-PNP, and adenosine are all mutually exclusive, as expected on the basis of the above binding studies, since they compete for the same specific adenosine binding pocket. On the other hand, there are interesting differences between the mixed-type patterns shown in panels B and E of Figure 3. While pyrophosphate and MgADP largely weaken inhibitions of each other, as indicated by the intercepting lines in the fourth quarter of the plot (Figure 3B), the same anion and MgAMP-PNP are closely additive inhibitors, and their effects are almost independent, as follows from the position of the interception close to the abscissa (Figure 3E). Similar results have also been obtained when (i) MgAMP-PCP was used in place of MgAMP-PNP or (ii) citrate was used in place of pyrophosphate (not plotted). Although the binding contribution of the phosphate chain of the Mg^{2+}−nucleotide complexes to the enzyme−substrate interaction is small (as indicated by the binding experiments described above), these kinetic studies suggest that the position of diphosphates of MgADP and that of triphosphates of the analogues of MgATP (and possibly of MgATP itself) may be different in the enzyme active site.

This interference of inhibitions by anions and MgADP, observed by us, has nothing to do with the anionic site [so-called "basic patch" (*70* and references therein)], which binds phosphate of the substrate 3-PG (*9*). Namely, similar double-inhibition experiments with a 3-PG analogue, 2-phosphoglycolate, in place of simple anions, gave different results: with both MgADP (Figure 3C) and MgAMP-PNP (Figure 3F) the lines intercept in the third quarter of the plot and close to the abscissa, indicating only a slight mutual influence of the two inhibitors. Thus, multiple inhibitory anion binding sites may exist in the active center, in agreement with crystallographic data, that allowed observation of a bound phosphate ion in the assumed 1-phosphate site of the other substrate, 1,3-BPG (*19*).

Protecting Effect of the Nucleotides against Unfolding. Stabilization of the protein structure in the enzyme substrate complexes is a well-known phenomenon. Protection against heat inactivation (*58*) and thermal unfolding (*71*) of PGK by its substrates have been noted. Here we investigated whether the differences (shown above) between interactions of MgATP and MgADP with PGK are reflected in their different stabilization effects on the enzyme structure. For this reason, the characteristic melting temperature (T_m) has been determined in DSC experiments, in the absence and presence of saturating concentrations of the nucleotides, as well as in the absence and presence of Mg^{2+}.

In the absence of Mg^{2+}, the protective effects of ATP and ADP are very similar: both ligands increase the T_m of PGK by 2.7 ± 0.3 °C (cf. the points on the ordinate of Figure 4 at an Mg^{2+} concentration of zero). Since we found that Mg^{2+}

itself induces instability in PGK, accompanied by a relatively large decrease in T_m (possibly due to weak unspecific binding to PGK), all measurements with the nucleotides were carried out in the presence of various concentrations of excess Mg^{2+}. To take into account this reverse effect of Mg^{2+}, the results are plotted in Figure 4 as a function of the free Mg^{2+} concentration (uncomplexed with the nucleotides) and fitted to eq 8. In this way, the experimental points could be extrapolated to an Mg^{2+} concentration of zero; i.e., the characteristic T_m values in the presence of saturating concentrations of MgATP and MgADP (which could not be measured directly) could be determined without the destabilization effect of Mg^{2+}. This procedure has revealed that the protecting effect of MgATP on the protein structure, at least within the experimental error, cannot be distinguished from that of ATP or ADP, while MgADP causes a further increase of ~1.9 °C in the melting temperature. Experiments with the ATP analogue AMP-PNP and MgAMP-PNP (not shown) gave T_m values very similar to those obtained with ATP and MgATP; i.e., in contrast to the pair of ADP and MgADP, the metal complexes of the nucleotide triphosphates apparently do not increase the protein stability compared to their metal-free forms. In other words, Mg^{2+} makes no special contribution to the stability when coordinated to nucleotide triphosphates; i.e., in these cases, the stability is resident in the nucleotide−protein interaction alone. Thus, the results indicate Mg^{2+} caused differences in the interactions of nucleotide diphosphate and triphosphate substrates with PGK, consistent with the structural data presented below.

Protecting Effect of the Nucleotides against Modification of the Reactive Thiols. Previous studies have shown that the reactivity of two thiol groups of pig muscle PGK, located in helix 13 (Cys377 and Cys378), is sensitive to the presence of all the bound substrates, among them MgATP and MgADP. This is possibly due to their effects on the local conformational flexibility around these thiols (*20*, *35*). Notable differences have been also observed. MgADP exerts much more protection than MgATP against modification of these reactive thiols with different reagents (*20*). Here we have investigated whether the different effects of the two nucleotides prevail or are abolished in the absence of Mg^{2+}. For this purpose, we have determined the reactivity of these thiols at saturating concentrations of ATP and ADP by modifying them with iodoacetamide. In control experiments, the substrate-free enzyme and the complexes with MgATP and with MgADP were reexamined. In addition, the effects of the ATP analogues (AMP-PNP and AMP-PCP) and the analogues containing a shorter phosphate chain (AMP) or having no phosphates (adenosine and adenine) have been studied. The second-order rate constants of thiol modification and their ratios are summarized in Table 4. It is remarkable that in the absence of Mg^{2+} all the phosphate-containing analogues protect the thiols similarly against modification, and this effect is not much larger than that of adenosine, which lacks phosphate. On the other hand, in the presence of Mg^{2+} only MgADP exerts an extremely large protection, as also noted earlier (*20*, *35*), compared to the much smaller protecting effects of MgATP, MgAMP-PNP, and MgAMP-PCP. Their effects are more or less similar to each other, but still significantly higher than those of their counterparts in the absence of Mg^{2+} or that of AMP. Mg^{2+} only slightly increases the effect of AMP in correlation with its relatively weak binding to the nucleotide monophosphate (*72*).

Table 4: Protective Effects of Various Bound Nucleotides against Modification of PGK Thiols by Iodoacetamide[a]

ligand (saturating)	no Mg		25 mM Mg^{2+}	
	k (M^{-1} s^{-1})	relative k	k (M^{-1} s^{-1})	relative k
none	0.1180 ± 0.017	1	0.1180 ± 0.017	1
ADP	0.0253 ± 0.0007	0.214	0.0013 ± 0.00018	0.011
ATP	0.0265 ± 0.0053	0.228	0.0140 ± 0.0025[b]	0.12
AMP-PCP	0.0296 ± 0.0014	0.25	0.0107 ± 0.0018	0.091
AMP-PNP	0.0280 ± 0.0019	0.24	0.0104 ± 0.0012	0.088
AMP	0.0287 ± 0.0007	0.243	0.0648 ± 0.0018	0.222
adenosine	0.0381 ± 0.0076[b]	0.32	–	–
adenine	0.1170 ± 0.254[b]	1	–	–

[a] PGK (1 μM) was reacted with various concentrations of iodoacetamide in the range of 10−60 mM in the absence and presence of each nucleotide at 10 mM. The time course of the reaction was fitted to a second-order rate equation. All rate constants have been normalized to the value determined in the absence of ligand. The results of experiments with Mg complexes were taken from ref *20*. [b] From ref *35*.

In summary, Mg^{2+}-induced characteristic differences among binding of various nucleotides to PGK are reflected by the thiol reactivity studies. It is notable that this method (which, in principle, measures the local accessibility of the reactive thiols) may be more sensitive in detecting differences in the binding modes of ATP and MgATP than DSC experiments, which reflect the stability of the whole protein molecule.

Crystal Structures of the Binary Complexes with ATP and MgATP. Cocrystallization of pig muscle PGK complexes with ATP and MgATP has allowed the determination of high-resolution crystal structures of these complexes (for details, cf. Materials and Methods and Table 1), which revealed interesting differences in the binding mode of nucleotide phosphates, depending on the absence or presence of Mg^{2+}.

The overall conformation of the enzyme molecule in these binary complexes is very similar and represents an essentially open position of the two domains (Figure 5A). This is expected on the basis of the possible occurrence of domain closure only in the ternary enzyme−substrate complexes, i.e., upon the synergetic action of both substrates (*11*). The structures presented here are even more open than the previously determined open structures of either the MgAMP-PCP·3-PG (*20*) (Figure 5B) or the MnAMP-PNP·3-PG (*17*) complex of pig muscle PGK. In the latter cases, the small extent of domain closure can be attributed to the bound 3-PG, but complete domain closure was prevented by the characteristic forces operating within the crystal lattice (*73*).

The nucleotide ATP or MgATP, like the previously described nucleotide-containing complexes (*7*, *13*, *17*, *20*), binds to the known adenosine binding pocket on the C-terminal domain. However, the direction and the geometry of their phosphates are remarkably different, not only from each other (cf. Figure 5A) but also, as shown below, from other known nucleotide conformations. Another remarkable feature of the ATP-containing structure is a single bound phosphate ion (shown also in Figure 5A) at the site, where otherwise the 3-phosphate group of 3-PG is bound (*9*).

The electron density maps for both ATP (Figure 6A) and MgATP (Figure 6B) clearly define the position of most of

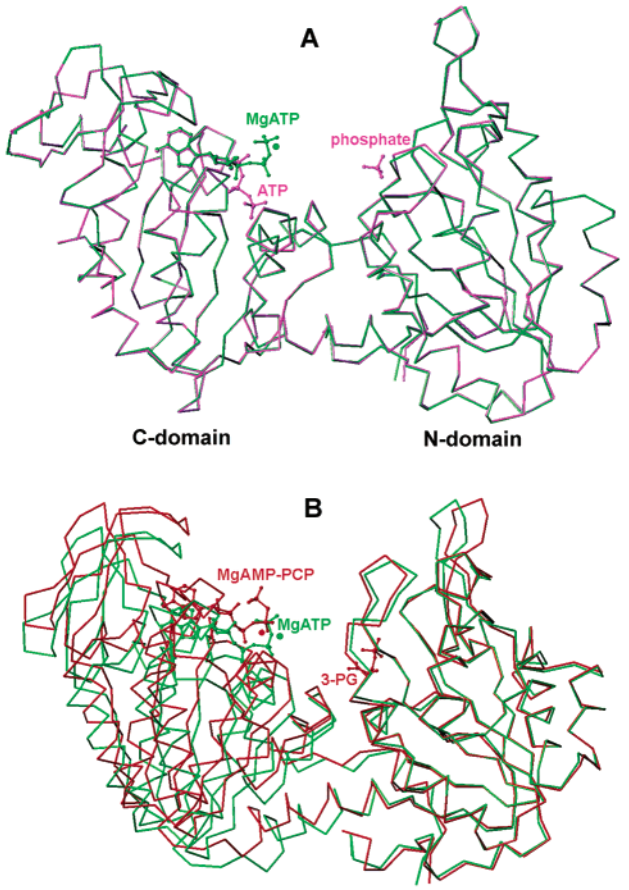

FIGURE 5: Comparison of the overall conformations of PGK in various complexes with nucleotides. The Cα traces of PGK structures with the ball-and-stick models of the bound ligands are shown: the present binary complexes with ATP (violet) and with MgATP (green) as well as the ternary complex with MgAMP-PCP and 3-PG (red) (*20*). The structures were superimposed according to the backbone atoms of the core β-strands of either the C-domain (A) or the N-domain (B).

the protein side chains, as well as the nucleotide positions. The characteristic interactions of ATP and MgATP with PGK are shown in panels C and D of Figure 6, respectively.

In the absence of Mg^{2+}, the phosphate chain of ATP is directed toward helix 13 and the γ-phosphate oxygen atoms are stabilized by multiple H-bonds to the main chain N atoms of Asp374 and Thr375 of this helix, as well as by the electrostatic interaction with the positive end of helix dipole at its N-terminus. Furthermore, an oxygen atom of the γ-phosphate also forms an H-bond with ND2 of the conserved Asn336, belonging to β-strand J, which is, in turn, H-bonded, through a water molecule (Wat479) to Gly372 O. Since the latter residue is also situated at the N-terminus of helix 13, this H-bond network strengthens the link of the γ-phosphate here. The β-phosphate is bound to a water molecule (Wat569), which is linked to two main chain O atoms of Gly212 and Asn336 (for clarity, the latter H-bond is not shown in Figure 6C). The β-phosphate also interacts with the side chain of the conserved Lys219 in the figure, but in the structure presented here, this side chain also occupies an alternative position with equal occupancy and interaction with the α-phosphate is formed (not shown), which is a known interaction in various PGK·nucleotide complexes (*7*, *13*, *17*, *20*).

The position and interactions of the MgATP phosphates are remarkably different from those of ATP. The γ-phosphate is positioned far from helix 13 and moved closer to the N-terminus of helix 8, although no interactions are formed with it; only a water molecule (Wat470) forms an H-bond with an oxygen atom of the γ-phosphate. On the other hand, an O atom of the β-phosphate is liganded (through Wat535) to the side chain of Asp218 at the N-terminus of helix 8. The position of Mg^{2+} with its characteristic interaction distances (*74*) is well-defined in the structure: it is complexed with O atoms of both β- and γ-phosphates, but does not interact directly with the protein. The α-phosphate is involved here in an interaction with the side chain of Lys219, known from previous structures with MgADP (*7*), MnAMP-PNP (*17*), MgAMP-PNP (*13*), and MgAMP-PCP (*20*).

An interesting feature of both structures is that the side chain of the conserved Lys215 exhibits a considerable flexibility, indicated by the low electron density in this region. The distances between its last resolved atom (CG) in the MgATP-bound structure (cf. Figure 6D) from Wat470, from O1G of the γ-phosphate, and from O1A of the α-phosphate are 4.88, 5.84, and 4.22 Å, respectively.

It is also notable that the *B*-factor values of the nucleotide phosphates vary between 57 and 67 $Å^2$ in both structures, similar to the value of 63 $Å^2$ found previously in the case of the bound MgAMP-PCP (*20*). This provides an argument in favor of the increased mobility of the nucleotide phosphate chain in these structures, considering the full occupation of the nucleotides (proved by the low *B*-factors of the adenosine moieties).

DISCUSSION

From the investigations of solubilized PGK presented here and from crystallographic studies, a comprehensive picture of the interactions with both nucleotide substrates can be derived. The general characteristics are as follows: (i) 1:1 stoichiometry of binding, (ii) dependence of the binding mode on complexation with Mg^{2+}, and (iii) significantly different interactions of MgATP and MgADP with PGK.

In the absence of Mg^{2+}, a highly ionic, possibly nonspecific interaction of ATP or ADP dominates between the uncompensated negative charges of their phosphates and the positively charged surface elements of PGK. The ionic character of the interaction follows from extensive displacement of the nucleotides by anions (Figure 2C), from the large negative value of the binding enthalpy (Δ*H* in Table 2), and from multiple interactions of ATP phosphates observed in the crystal structure (Figure 6C). In addition, the partial displacement by adenosine (Figure 2A) provides an argument against the exclusive occupation of the adenosine binding pocket.

In contrast, both MgATP and MgADP bind solely to the adenosine binding site, as expected for the nucleotide substrates, which was clearly indicated both by the purely competitive displacement by adenosine (Figure 2B) and by the presently (Figure 6D) and previously (e.g., Figure 7C) determined crystal structures. However, significant differences have been observed in both the geometry and interactions of phosphates of MgATP and MgADP with the protein both in the crystal structures (compare Figure 6D to Figure 7C) and in the solution phase experiments presented here.

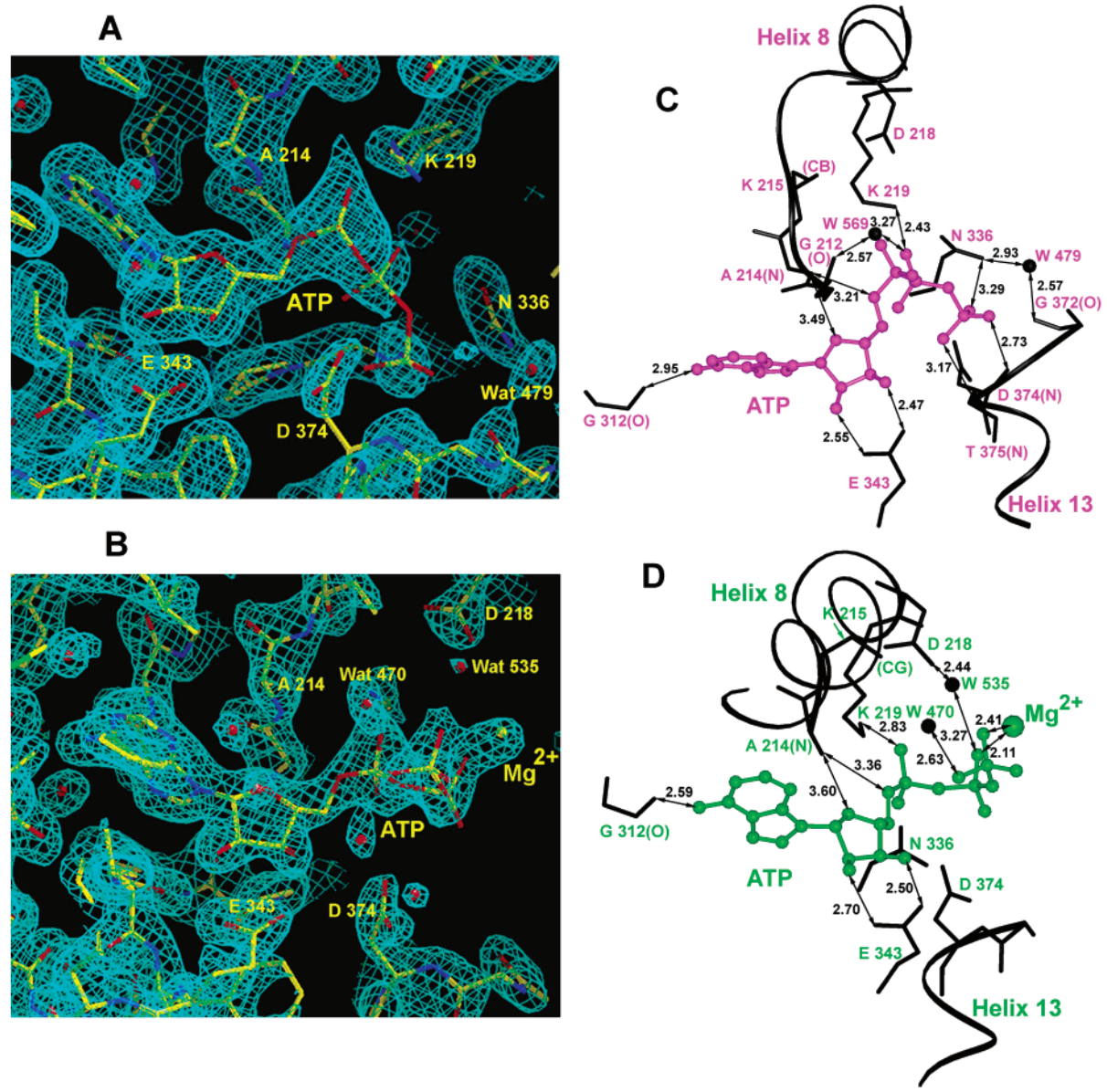

FIGURE 6: Structural details of the interactions of PGK with ATP and MgATP. Electron density maps of the nucleotide site, contoured at 1.0σ with bound ATP (A) and at 1.3σ with bound MgATP (B), as well as the ball-and-stick models of the nucleotides colored violet for ATP (C) and green for MgATP (D), together with their surrounding residues (stick models) and helices (ribbons), colored in black. Only one of the two alternative positions of Lys 219 side chain is denoted in panel C. The distances are indicated in angstroms.

Namely, MgATP lacks the stabilization effect of Mg^{2+} observed in the case of MgADP binding; i.e., the ionic interaction of MgADP phosphates with the conserved aspartate carboxylate (Asp377 in *Trypanosoma brucei* PGK, Figure 7C) of helix 13 is lacking in binding of MgATP (Asp374 in pig muscle PGK, Figure 6D). This is supported by (i) different K_d values and thermodynamic parameters of binding (Tables 2 and 3), (ii) different inhibitory kinetic patterns with the MgATP analogue (MgAMP-PNP) and with MgADP (Figure 3), and (iii) a much smaller stabilization effect of MgATP, compared to that of MgADP, on the protein structure, as detected by DSC calorimetry (Figure 4) or by measuring the reactivity of the thiol groups (Table 4) located in helix 13, close to the known main hinge, the conformation of which is sensitive for substrate binding (*9*, *10*, *20*). As shown (*9*, *10*, *20*), these thiols are more reactive when helix 13 is less ordered. In fact, the average crystallographic *B*-factor of the backbone atoms of helix 13 is larger in the MgATP binary complex described herein (40.5 Å^2) than the values of either 26.8 or 31.1 Å^2 observed previously for the MgADP binary complex (*7*) or the MgADP-containing ternary complex (*19*), respectively. These data corroborate the smaller protection against thiol modification by the bound MgATP, compared to the large protection by MgADP.

A related characteristic is the greater flexibility of the bound MgATP phosphates (the average *B*-factor is 62.8 Å^2), compared to the phosphates of MgADP [the *B*-factors are 16.7 (*7*) and 30.27 Å^2 (*19*)]. Most probably, complexation with the metal ion affects differently the phosphate chain flexibility of MgATP and MgADP. In contrast to MgADP, Mg^{2+} interacts with only the nucleotide, and not with any protein atoms; therefore, complex formation with the metal ion does not restrict the mobility of MgATP phosphates. The mainly entropy-driven binding of MgATP, as revealed by calorimetric titration (Table 2), although it does not prove

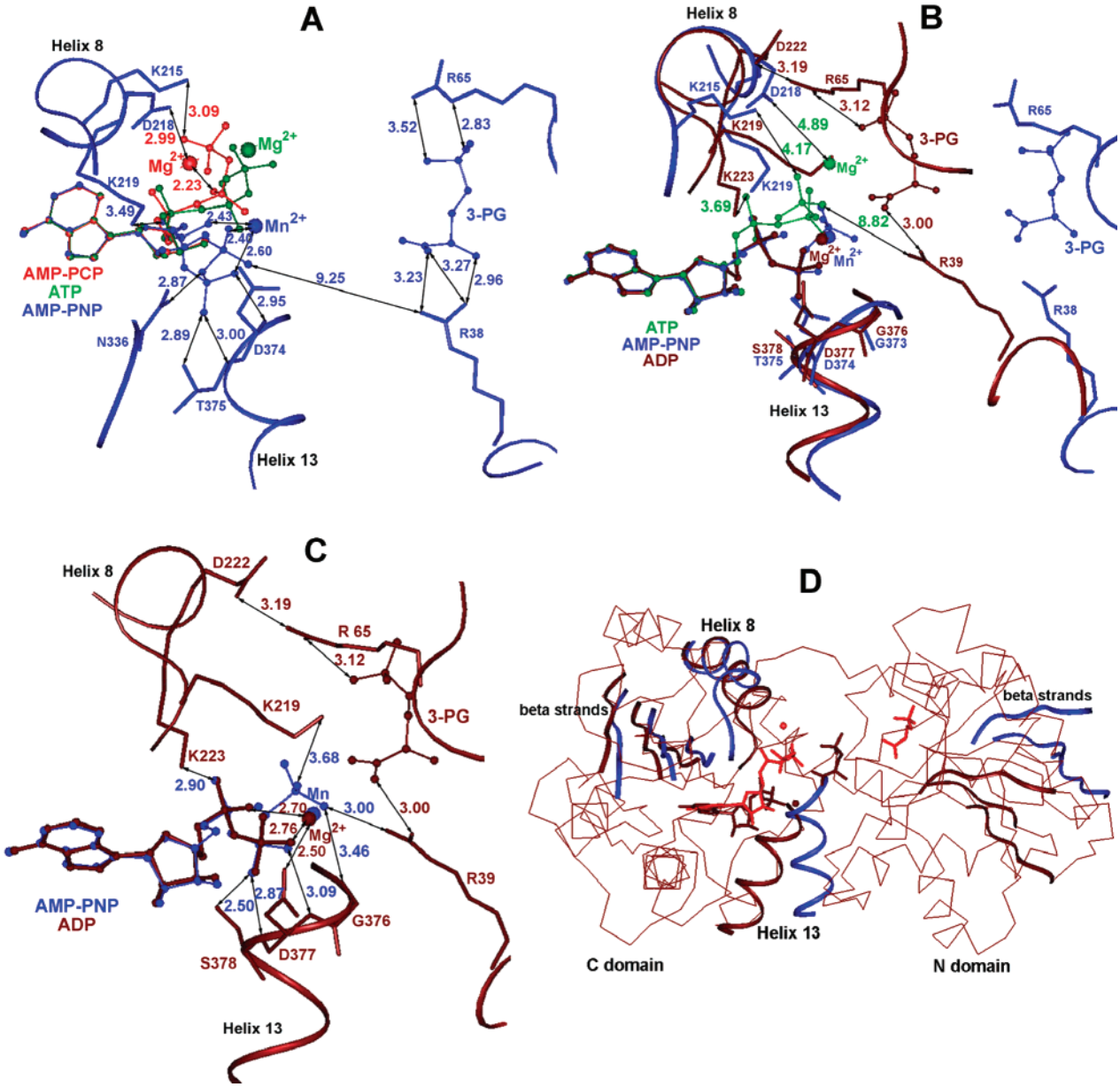

FIGURE 7: Illustration of the possible catalytic role of phosphate chain movement of MgATP. The present MgATP (green), the previous MgAMP-PCP·3-PG (*20*) (red), and MnAMP-PNP·3-PG (*17*) (blue) complexes of pig muscle PGK as well as the MgADP·3-PG (brown) complex of *T. brucei* PGK (*19*) were superimposed according to all atoms of the adenosine rings of the bound nucleotide in panels (A−C). Substrates are depicted as ball-and-stick models, while stick models represent selected residues or side chains. Labeling of the side chains follows the color code, and the numbering is characteristic of each PGK sequence. Selected atomic distances, denoted with arrows, are given in angstroms. In panel A, MgAMP-PCP (red) and MgATP (green) are superimposed onto the structure of the open conformation of pig muscle PGK containing bound MnAMP-PNP and 3-PG (blue). In panel B, the closed conformation of the *T. brucei* MgADP·3-PG complex (brown) is superimposed onto the open conformation of pig muscle PGK MnAMP-PNP·3-PG complex (blue) and the bound MgATP (green) is also shown. Panels C is the same as panel B, except the protein surroundings of the bound MnAMP-PNP (blue) are omitted. It is notable that the conformation of MgAMP-PNP, as it binds to the closed structure of *T. maritima* PGK (*13*) (not shown), is only hardly distinguishable from that of MnAMP-PNP (blue) bound in the structure of pig muscle PGK. The same is valid when the conformation of MgADP, as it binds to *B. stearothermophilus* PGK (*7*), is compared to the MgADP conformation (brown) bound to *T. brucei* PGK, shown here. Panel D shows the Cα trace of the closed conformation of the whole *T. brucei* PGK molecule (brown) together with the bound MgADP and 3-PG (brown). The open conformation of the pig muscle PGK molecule (blue) together with the bound MgAMP-PCP and 3-PG (red) is superimposed onto the closed structure according to the backbone atoms of helix 8. For clarity, the Cα trace of pig muscle PGK is not shown. Parts of both PGKs (helices 8 and 13, as well as the core β-strands of each domain) are highlighted as ribbons.

itself, is in accordance with the flexible phosphate chain of the bound MgATP.

The conformation and orientation of MgATP phosphates observed in the structure presented here (green) are different from those characteristic either of the metal complexes of AMP-PNP (blue) (*13*, *17*) or of AMP-PCP (red) (*20*) (cf. Figure 7A). In light of the mobility of MgATP phosphates, this figure may suggest a considerable variation of the conformation of the bound nucleotide triphosphate. Thus, one may assume that these phosphates can fluctuate between two alternative positions, which was originally observed in separate crystal structures with MgAMP-PCP (*20*) and MnAMP-PNP (*17*). Since the crystal represents a rigid structure, one usually observes only one of the alternative

geometries, depending on the crystallization conditions. There are the following arguments for the assumed fluctuation. (i) The binding geometries of AMP-PNP and of AMP-PCP in the solution phase are similar, since both compounds behave similarly as ATP analogues in the double-inhibition experiments (Figure 3). (ii) The effects of ATP, AMP-PNP, and AMP-PCP (either in their free form or in Mg^{2+} complexes) are very similar both on PGK stability (Figure 4) and the local conformational flexibility around the reactive thiols (Table 4), indicating their similar interaction with PGK.

On this basis, we put forward the following proposal concerning the catalytic mechanism. The open active site of PGK, as illustrated by the crystal structure (blue in Figure 7A) of the complex of pig muscle PGK with MnAMP-PNP and 3-PG (*17*), can accommodate the conformations of either MgATP (green, from the structure presented here) or MgAMP-PCP (red, from ref *20*). In fact, an O atom of the γ-phosphate of MgAMP-PCP is within H-bonding distance of Lys215 (NZ), and Mg^{2+} is at an almost ideal distance for the interaction with the carboxylate of Asp218, similar to the interactions of MgAMP-PCP identified in the original crystal structure of its complex. We assume that in place of MgAMP-PCP, the γ-phosphate of MgATP can equally occupy this position and bind to this alternative phosphate site. Figure 7A shows the active site of the inactive open conformation of PGK, as indicated by the large distance between the reactive groups of the substrates. In the ternary complex in solution, containing both MgATP and 3-PG, a mechanism of domain closure is operating [its details and location of hinges have been discussed elsewhere (*10*, *11*)]. In the course of domain closure, Arg65, which (among other arginine residues) participates in binding of 3-PG, moves closer to Asp218 [equivalent to Asp222 in the closed conformation of *T. brucei* PGK with bound MgADP and 3-PG (*19*); brown in Figure 7B], displaces the interacting Mg^{2+}, and forms a salt bridge with Asp218. This salt bridge has been assumed to stabilize the closed conformation (*13*). The interaction of Mg^{2+} with the protein is thereby suspended, and it moves away together with the interacting phosphates of MgATP. This intermediate conformation and position of phosphates may be illustrated by the structure of the bound MgATP (green in Figure 7B). While the nucleotide phosphates move farther, there is no reason to suspend the originally formed interaction with the side chain of Lys215 (equivalent with Lys219 in *T. brucei* PGK). Thus, this side chain, which is located at the N-terminus of helix 8, most probably, moves together with the interacting phosphate. A movement of more than 5 Å of this Lys side chain is illustrated by the superimposed open (*17*) and closed (*19*) structures in Figure 7B. This movement is accompanied by a movement of ~7 Å of the nucleotide γ-phosphate, and in this way, MgATP may finally occupy the position and take the phosphate chain conformation that is characteristic of the metal complex of AMP-PNP. This is pictured in Figure 7C, where only the bound MnAMP-PNP [blue, taken from the open structure of pig muscle PGK (*17*)] is superimposed with MgADP (brown) bound in the closed active site of *T. brucei* PGK (*19*). It is notable that the conformations and the interactions of the phosphates of the nucleotide triphosphate with the enzyme (mainly with helix 13) are almost identical with those of MgADP (brown), except for the presence of γ-phosphate and for the interactions of Mg^{2+}. One can postulate that this position of the γ-phosphate is the catalytic position of the phospho group transferred from MgATP, since it is stabilized by the interacting Lys219 and Arg39 (equivalent to Lys215 and Arg38 in pig muscle PGK), as well as by a possible link (indicated by a weak H-bond in Figure 7C) to Gly376 N (equivalent to Gly373 at the N-terminus of helix 13) and a distance of 2.81 Å from an O atom of the γ-phosphate to Gly399 N (not shown, equivalent to Gly396 at the N-terminus of helix 14).

Stabilization of the transferring phospho group by exactly the same interactions has been deduced in another way, solely from the crystal structure of *T. brucei* PGK (*19*). In this proposal, we additionally assume a movement of Lys215 (belonging to helix 8), as a key element, induced by the interacting mobile phosphates of MgATP. This is an interesting example of substrate-assisted construction of the proper geometry of an enzyme active site for catalysis. Movement of Lys215 not only finalizes the formation of the catalytic site but also at the same time contributes to the movement of helix 8 (to which it belongs) relative to helix 13 (cf. Figure 7D), and the domain closure is thereby also facilitated, in line with its suggested mechanism (*10*). The mobility of MgATP phosphates may be coupled with the mobility of the surrounding side chains. In fact, a considerable mobility of the conserved Lys215 has been observed in both the structure with MgATP presented here and the previously published structure with MgAMP-PCP (*20*).

MgADP cannot fulfill a similar role in the active site closure as suggested above for MgATP, considering its unique binding mode, the strong link of its phosphates, and the complexing of Mg^{2+} to helix 13. Instead, a different mechanism may operate. We propose the fluctuation of the 1-phosphate group of 1,3-bisphosphoglycerate (1,3-BPG) between two alternative anionic sites, similar to that of MgATP. Although no structural information exists for the complex with this substrate, it is reasonable to assume its binding in the known site of 3-PG. A phosphate ion was actually observed to bind very close to the known position of 3-PG carboxylate, i.e., in a possible place for the 1-phosphate of 1,3-BPG in the closed conformation of *T. brucei* PGK (*19*). Bernstein and Hol (*19*) have shown that this phosphate is just in the right position (stabilized by the same interactions with protein as shown above) for the transfer; thus, this structure of *T. brucei* PGK can be the catalytic complex with 1,3-BPG and MgADP. In the open conformation, however, one may imagine an alternative binding mode, consistent with the size and geometry of 1,3-BPG, in which its two negatively charged phosphates would span the gap of ~12−13 Å between the positively charged groups of Lys215 (C-domain) and Arg65 (N-domain) (pig muscle PGK numbering). These initial interactions would facilitate the movement of the side chain of Lys215 into its right place in the closed conformation of the catalytic complex. At present, we have no evidence in favor of this hypothesis, except recent kinetic studies of the forward and reverse directions of the PGK reaction, which have revealed that the optimal factors of the active site environment for MgADP or MgATP as substrates are pronouncedly different (*75*).

In summary, the flexible phosphate chain of MgATP may possess a considerable level of mobility and fluctuates between two alternative sites existing in the inactive open

conformation of PGK. This fluctuation may be an essential element of the catalytic cycle, since by this way the nucleotide substrate itself would assist in formation of the catalytically competent closed active site. In the reverse reaction, Mg^{2+} links the phosphates of MgADP to the protein and thereby ensures its fixed position to accept the transferred phospho group. In this reaction, the 1-phosphate of 1,3-BPG (in place of the γ-phosphate of MgATP) might be responsible for construction of the properly closed catalytic site.

ACKNOWLEDGMENT

Thanks are due to A. Merli (Institute of Biochemical Sciences, University of Parma, Parma, Italy) for providing the crystal growing facilities and to V. Harmat (Protein Modeling Group, Hungarian Academy of Sciences-Eötvös Loránd University) for helping in the crystallographic data processing.

REFERENCES

1. Larsson-Raznikiewicz, M. (1964) *Biochim. Biophys. Acta 85*, 60−68.
2. Larsson-Raznikiewicz, M. (1967) *Biochim. Biophys. Acta 132*, 33−40.
3. Larsson-Raznikiewicz, M. (1970) *Eur. J. Biochem. 17*, 183−192.
4. Knowles, J. R. (1980) *Annu. Rev. Biochem. 49*, 877−919.
5. Herschlag, D., and Jencks, W. P. (1990) *Biochemistry 29*, 5172−5179.
6. Tari, L. W., Matte, A., Goldie, H., and Delbaere, L. T. (1997) *Nat. Struct. Biol. 4*, 990−994.
7. Davies, G. J., Gamblin, S. J., Littlechild, J. A., Dauter, Z., Wilson, K. S., and Watson, H. C. (1994) *Acta Crystallogr. D50*, 202−209.
8. Banks, R. D., Blake, C. C. F., Evans, P. R., Haser, R., Rice, D. W., Hardy, G. W., Merrett, M., and Phillips, A. W. (1979) *Nature 279*, 773−777.
9. Harlos, K., Vas, M., and Blake, C. C. F. (1992) *Proteins 12*, 133−144.
10. Szilágyi, A. N., Ghosh, M., Garman, E., and Vas, M. (2001) *J. Mol. Biol. 306*, 499−511.
11. Bernstein, B. E., Michels, P. A. M., and Hol, W. G. J. (1997) *Nature 385*, 275−278.
12. Geerlof, A., Schmidt, P. P., Travers, F., and Barman, T. (1997) *Biochemistry 36*, 5538−5545.
13. Auerbach, G., Huber, R., Grättinger, M., Zaiss, K., Schurig, H., Jaenicke, R., and Jacob, U. (1997) *Structure 5*, 1475−1483.
14. Pickover, C. A., McKay, D. B., Engelman, D. M., and Steitz, T. A. (1979) *J. Biol. Chem. 254*, 11323−11329.
15. Sinev, M. A., Razgulyaev, O. I., Vas, M., Timchenko, A. A., and Ptitsyn, O. B. (1989) *Eur. J. Biochem. 180*, 61−66.
16. Watson, H. C., Walker, N. P. C., Shaw, P. J., Bryant, T. N., Wendell, P. L., Fothergill, L., Perkin, R. E., Conroy, S. C., Dobson, M. J., Tuite, M. F., Kingsman, A. J., and Kingsman, S. M. (1982) *EMBO J. 1*, 1635−1640.
17. May, A., Vas, M., Harlos, K., and Blake, C. C. F. (1996) *Proteins 24*, 292−303.
18. McPhillips, T. M., Hsu, B. T., Sherman, M. A., Mas, M. T., and Rees, D. C. (1996) *Biochemistry 35*, 4118−4127.
19. Bernstein, B. E., and Hol, W. G. (1998) *Biochemistry 37*, 4429−4436.
20. Kovári, Z., Flachner, B., Náray-Szabó, G., and Vas, M. (2002) *Biochemistry 41*, 8796−8806.
21. Larsson-Raznikiewicz, M. (1973) *Arch. Biochem. Biophys. 158*, 754−762.
22. Tanswell, P., Westhead, E. W., and Williams, R. J. P. (1974) *FEBS Lett. 48*, 60−63.
23. Scopes, R. K. (1978) *Eur. J. Biochem. 91*, 119−129.
24. Wiksell, E., and Larsson-Raznikiewicz, M. (1987) *J. Biol. Chem. 262*, 14472−14478.
25. Nageswara-Rao, B. D., Cohn, M., and Scopes, R. K. (1978) *J. Biol. Chem. 253*, 8056−8060.
26. Ray, B. D., and Nageswara-Rao, B. D. (1988) *Biochemistry 27*, 5574−5578.
27. Ray, B. D., Moore, J. M., and Nageswara-Rao, B. D. (1990) *J. Inorg. Biochem. 40*, 47−57.
28. Fairbrother, W. J., Graham, H. C., and Williams, R. J. P. (1990) *Eur. J. Biochem. 190*, 407−414.
29. Graham, H. C., and Williams, R. J. P. (1991) *Eur. J. Biochem. 197*, 81−91.
30. Tanswell, P., Westhead, E. W., and Williams, R. J. P. (1976) *Eur. J. Biochem. 63*, 249−262.
31. Roustan, C., Brevet, A., Pradel, L. A., and Thoai, N. v. (1973) *Eur. J. Biochem. 37*, 248−255.
32. Wiksell, E., and Larsson-Raznikiewicz, M. (1982) *J. Biol. Chem. 257*, 12672−12677.
33. Vas, M., and Batke, J. (1984) *Eur. J. Biochem. 139*, 115−123.
34. Vas, M., Merli, A., and Rossi, G. L. (1994) *Biochem. J. 301*, 885−891.
35. Tompa, P., Hong, P. T., and Vas, M. (1986) *Eur. J. Biochem. 154*, 643−649.
36. Molnár, M., and Vas, M. (1993) *Biochem. J. 293*, 595−599.
37. Merli, A., Szilágyi, A. N., Flachner, B., Rossi, G. L., and Vas, M. (2002) *Biochemistry 41*, 111−119.
38. Chapman, B. E., O'Sullivan, W. J., Scopes, R. K., and Reed, G. H. (1977) *Biochemistry 16*, 1005−1010.
39. Ray, B. D., and Rao, B. D. (1988) *Biochemistry 27*, 5579−5585.
40. Moore, J. M., and Reed, G. H. (1985) *Biochemistry 24*, 5328−5333.
41. Jaffe, E. K., Nick, J., and Cohn, M. (1982) *J. Biol. Chem. 257*, 7650−7656.
42. Dunaway-Mariano, D., and Cleland, W. W. (1980) *Biochemistry 19*, 1506−1515.
43. Shibata, C. G., Gregory, J. D., Gerhardt, B. S., and Serpersu, E. H. (1995) *Arch. Biochem. Biophys. 319*, 204−210.
44. Lester, L. M., Rusch, L. A., Robinson, G. J., and Speckhard, D. C. (1998) *Biochemistry 37*, 5349−5355.
45. Raghunathan, V., Chau, M. H., Ray, B. D., and Rao, B. D. (1999) *Biochemistry 38*, 15597−15605.
46. Eöd, P., and Szörényi, E. (1956) *Acta Physiol. Acad. Sci. Hung. 9*, 339−350.
47. Burton, K. (1959) *Biochem. J. 71*, 388−395.
48. Miller, C., Frey, C. M., and Stuehr, J. E. (1972) *J. Am. Chem. Soc. 94*, 8898−8904.
49. Gupta, R. K., Gupta, P., Yashok, W. P., and Rose, Z. B. (1983) *Biochem. Biophys. Res. Commun. 117*, 210−216.
50. Zhang, W., Truttmann, A. C., Luthi, D., and McGuigan, J. A. (1997) *Anal. Biochem. 251*, 246−250.
51. Yount, R. G., Babcock, D., Ballantyne, W., and Ojala, D. (1971) *Biochemistry 10*, 2484−2489.
52. Krietsch, W. K., and Bücher, T. (1970) *Eur. J. Biochem. 17*, 568−575.
53. Fox, I. B., and Dandliker, W. B. (1956) *J. Biol. Chem. 221*, 1005−1017.
54. Szilágyi, A. N., and Vas, M. (1998) *Biochemistry 37*, 8551−8563.
55. Smith, R. M., and Martell, A. E. (1976) *Critical Stability Constans*, Inorganic Complexes Vol. 4. pp. 56−59, Plenum Press, New York, London.
56. Smith, R. M., and Martell, A. E. (1977) *Critical Stability Constans*, Other Organic Ligands Vol. 3. pp. 164−164, Plenum Press, New York, London.
57. Yonetani, T., and Theorell, H. (1964) *Arch. Biochem. Biophys. 106*, 243−351.
58. Cserpán, I., and Vas, M. (1983) *Eur. J. Biochem. 131*, 157−162.
59. Vas, M., and Csanády, G. (1987) *Eur. J. Biochem. 163*, 365−368.
60. Minard, P., Desmadril, M., Ballery, N., Perahia, D., Mouawad, L., Hall, L., and Yon, J. M. (1989) *Eur. J. Biochem. 185*, 419−423.
61. Riddles, P. W., Blakeley, R. L., and Zerner, B. (1983) *Methods Enzymol. 91*, 49−60.
62. Dékány, K., and Vas, M. (1984) *Eur. J. Chem. 139*, 125−130.
63. Finkle, B. J., and Smith, E. L. (1958) *J. Biol. Chem. 230*, 669−690.
64. Leslie, A. G. W. (1992) *Newsletter on Protein Crystallography 26*.
65. Navaza, J. (1994) *Acta Crystallogr. A50*, 157−163.
66. Collaborative Computational Project Number 4 (1994) *Acta Crystallogr. D40*, 760−763.
67. Brunger, A. T. (1992) *X-PLOR: Version 3.1; a system for protein crystallography and NMR*, Yale University Press, New Haven, CT.
68. Jones, T. A., Zou, J.-Y., Cowan, S. W., and Kjeldgaard, M. (1991) *Acta Crystallogr. A47*, 110−119.

69. Quackenbush, J., Liang, F., Holt, I., Pertea, G., and Upton, J. (2000) *Nucleic Acids Res. 28*, 141−145.
70. Joao, H. C., and Williams, R. J. P. (1993) *Eur. J. Biochem. 216*, 1−18.
71. Bentahir, M., Feller, G., Aittaleb, M., Lamotte-Brasseur, J., Himri, T., Chessa, J. P., and Gerday, C. (2000) *J. Biol. Chem. 275*, 11147−11153.
72. Ragot, M., Sari, J. C., and Belaich, J. P. (1977) *Biochim. Biophys. Acta 499*, 411−420.
73. Kovári, Z., and Vas, M. (2004) *Proteins 55*, 198−209.
74. Harding, M. M. (1999) *Acta Crystallogr. D55*, 1432−1443.
75. Krishnan, P., Liou, J. Y., and Cheng, Y. C. (2002) *J. Biol. Chem. 277*, 31593−31600.
76. Laskowski, R. A., MacArthur, M. W., Moss, D. S., and Thorton, J. M. (1993) *J. Appl. Crystallogr. 26*, 283−291.

BI035022N